Polyelectrolyte assisted interfacial polymerization for polyamide nanofiltration membrane with enhanced separation and anti-biofouling properties in groundwater treatment

Ying Mei[a,b *], Zhe Yang[b], Peng-Fei Sun[b,c], Shenghua Zhou[b], Hao Guo[b], Lu Elfa Peng[b], Zhikan Yao[b,d], Wulin Yang[b,e], Chuyang Y. Tang[b]

[a]*Research and Development Center for Watershed Environmental Eco-Engineering, Advanced Institute of Natural Sciences, Beijing Normal University, Zhuhai 519087, PR China*

[b]*Department of Civil Engineering, The University of Hong Kong, Pokfulam, Hong Kong SAR, PR China*

[c]*School of Civil, Environmental and Architectural Engineering, Korea University, Seoul 02841, South Korea*

[d]*MOE Engineering Research Center of Membrane and Water Treatment Technology, College of Chemical and Biological Engineering, Zhejiang University, Hangzhou 310027, PR China*

[e]*College of Environmental Sciences and Engineering, Peking University, Beijing 100871, PR China*

* Corresponding author address:

B504 Muduo Building, Beijing Normal University, Zhuhai,18 Jinfeng Road, Zhuhai, Guangdong, PR China.

Tel: (+86) 15034117623;

E-mail address: meiying@bnu.edu.cn (Ying Mei)

Abstract

We proposed a facile method of using polyelectrolyte additive to tune interfacial polymerization reaction and tailor polyamide NF membrane with better separation performance and lower bio-fouling potential for groundwater treatment. A moderate concentration of negatively charged poly(4-styrene sulfonate) (PSS) was introduced to the aqueous phase solution during the interfacial polymerization of piperazine (PIP) and trimesoyl chloride (TMC). The presence of PSS confined the diffusion of PIP, leading to the formation of polyamide layer with a looser structure, increased thickness, and additional negative charges on the membrane surface. The fabricated TFC-P_6 membrane possessed enhanced water permeance (21.8 ± 0.7 L m^{-2} h^{-1} bar^{-1}) and better selectivity of calcium chloride over sodium sulfate which can be beneficial to achieve higher water recovery compared to the control TFC membrane. In addition, the TFC-P_6 membrane demonstrated enhanced rejection of perfluorooctane sulfonate (~95%) and the biofouling was inhibited by its additional negative charge and smoother surface. Our results introduced a robust and scalable strategy of polyelectrolyte assisted interfacial polymerization for designing high performance NF membranes in groundwater treatment.

Keywords: Nanofiltration, Polyamide membrane, Interfacial polymerization, Polyelectrolyte, Biofouling

1. Introduction

Safety of drinking water generated from groundwater resources has been recognized as the main worldwide challenge. However, it has been widely contaminated by emerging contaminants which would threaten the public health even at low concentrations [1-6]. Among them, perfluoroalkyl substances (PFASs) present a diverse group of persistent, accumulative and toxic trace contaminants comprising perfluoroalkyl groups. They are extensively produced and commonly applied in manufacturing industrial products, such as fighting foams and protective coatings [7-9]. Although the usage of PFASs has been strictly regulated by many countries, its environmental concentrations are still noticeable (e.g., at the range of several ppt to ppm) [10, 11]. For example, perfluorooctane sulfonate (PFOS), one of the most commonly regulated PFASs, is ubiquitously detected with averaged concentrations up to a few ppt in the aquatic environments [11-13]. It is highly resistant to conventional chemical and biological wastewater treatment technologies, attributing to the strong carbon-fluorine bonds [14, 15]. Physical separation and sequestration processes, including membrane separation and adsorption, are mostly applied for removing PFOS from polluted water resources [3, 16].

Nanofiltration (NF) has been validated to be a promising membrane-based separation technology for treating PFOS contaminated water [3, 17, 18]. It can be operated in relatively low-pressure with a typical molecular weight cut off at the range of 200-1000 Da. NF separation is mainly based on the combined effects of size exclusion and electrostatic repulsion [8, 19-22]. PFOS has a relatively high molecular weight of 500 Da and is generally dissociated into negatively charged ion at natural waters that high retention rates of PFOS (e.g., ≥ 90%) were reported in previous researches [9, 17, 23]. Nevertheless, the practical

implementation of NF for PFASs contaminated groundwater resources is still inhibited by its limited water recovery (e.g., 75-80%) due to potential membrane scaling and bio-fouling problems [8]. Polyamide (PA) based thin film composite membranes are dominant NF membranes of which the PA rejection layer is normally fabricated by interfacial polymerization (IP) of piperazine (PIP) and trimesoyl chloride (TMC) at aqueous and organic interface and have an averaged pore size of 0.2-2 nm. The TFC NF membranes can well retain scale-forming ions (e.g., Ca^{2+}, Mg^{2+}, SO_4^{2-} etc.), leading to severe concentrating of these ions and precipitation of scalant on membrane surface, especially at high water recovery. On the other hand, mineral ions in drinking water resources would be favorable for human body and agricultural crops and should be retained in the permeate. In addition, membrane bio-fouling is another critical concern of NF technology which would also deteriorate membrane separation performance [24-26]. Therefore, developing novel NF membranes is of critical importance to realize the asymmetric selectivity of mineral ions toward reduced scaling potential and less bio-fouling risks while maintaining high PFOS rejection. Previous research has presented a membrane design with increased pore size and surface negative charges that provides enhanced anti-scaling property and high rejection of PFOS [27]. It was realized by tailoring a loose PA layer through incorporating NaOH into the aqueous solution during IP reaction. Recently, another facile method of controlling the reaction-diffusion IP process has attracted people's attention that nonreactive additives of aqueous phase, such as macromolecule and amphiphilic surfactant, can regulate the trans-interface diffusion of aqueous monomer by hydrogen bonding, changing solution viscosity and electrostatic interaction, thus determining the IP reaction process [28].

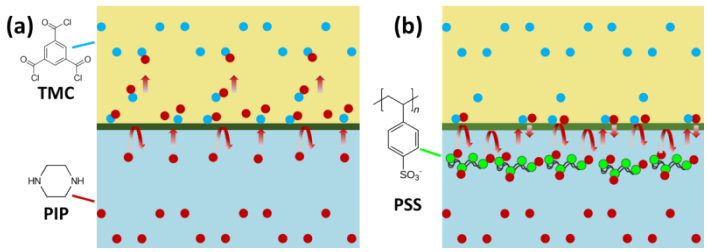

Fig. 1. Schematic diagram illustrating diffusion process of (a) the conventional IP reaction where piperazine molecules diffuse randomly through the interface between water and hexane and (b) negatively charged PSS assisted IP reaction where PIP molecules are adsorbed by PSS and diffuse in the more controllable manner.

In this study, we proposed a simple anionic polyelectrolyte assisted IP reaction for fabricating a loose and negatively charged TFC NF membrane toward high selectivity for calcium over sulfate and high rejection of PFOS while less bio-fouling occurred. Poly(sodium-4-styrene sulfonate) (PSSNa) was applied as the model anionic polyelectrolyte additive for PIP/water solution due to its wide commercial availability. We envisioned that this negatively charged macromolecule is able to slow-down the PIP diffusion via electrostatic interaction and regulate the distribution of PIP monomer at the interface, thus obtaining PA layer with more homogeneous distribution of large pores compared to conventional TFC membranes (Fig. 1). Varied concentrations of PSSNa additives were investigated for their impacts on the physicochemical properties and the separation performance of PA layer. The virgin and modified membranes were evaluated for their performance in selectively rejection of inorganic salts and PFOS. Finally, the biofouling experiments were performed on both virgin and modified membranes to comparatively investigate their anti-biofouling behaviors. This study presents a simple and facile method of tailoring NF membrane for PFAS contaminated groundwater treatment at higher freshwater recovery and with decreased biofouling phenomenon.

2. Materials and methods

2.1. Materials and reagents

Polysulfone (PSf, Mw 35000, Sigma-Aldrich) dissolved in N,Ndimethylformamide (DMF, 99.8%, Sigma-Aldrich) were applied for membrane substrates preparation. PIP (flakes, 99%, Sigma-Aldrich) in deionized (DI) water and TMC (98%, Sigma-Aldrich) in *n*-hexane (≥ 95%, HPLC grade, Sigma-Aldrich) were applied for interfacial polymerization reaction to synthesize PA rejection layer on the PSf support. PSSNa (MW ~70,000 Da, Sigma-Aldrich) was chosen as the model PIP/water solution additive in the current study. Inorganic salts, including NaCl, Na_2SO_4, $MgCl_2$, $MgSO_4$, and $CaCl_2$ were all provided by Uni-Chem. Neutral organic molecules, including D-Glucose (MW 180 Da, Coolaber), D-raffinose (MW 504 Da, Aladdin), dextran (MW 1000 Da, OKA), and (MW 2000 Da, OKA) were applied to test membrane rejection for its pore size estimation. PFOS was supplied by Sigma-Aldrich. Invitrogen™ DAPI (4',6-Diamidino-2-Phenylindole, Dihydrochloride) was used to stain the biofilm for fluorescent observation.

2.2. TFC and TFC-P_n membranes preparation

The synthesis of PSf substrate was completed using a nonsolvent-induced phase separation technique based on our previous study [29, 30]. Briefly, an automatic film applicator (Elcometer 4340, Elcometer) was used to spread a PSf solution (15 wt.% in DMF) onto a glass plate with a controlled thickness of 150 μm. Subsequently, the PSf substrate was immersed in a water coagulation bath at about 25°C. Finally, the obtained substrates were rinsed and stored in DI water before further use.

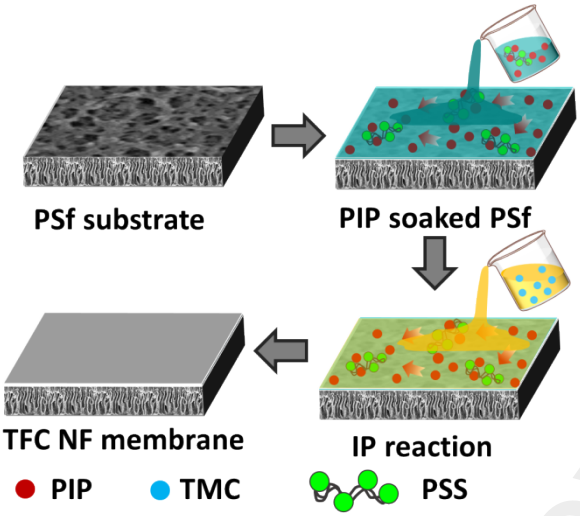

Fig. 2. Schematic diagram illustrating PSS assisted interfacial polymerization for the synthesis of polyamide thin film composite nanofiltration membrane.

As reported in our previous study, interfacial polymerization (IP) was performed on the PSf support to form the PA rejection layer [30, 31]. PIP/water solution (2 wt.%) without and with PSSNa additives of varied concentrations (i.e., 0.2, 2, 6, 12 wt.%) were prepared to investigate the role of anionic polyelectrolyte on PA formation (Fig. 2). To synthesis the PA layer, a PSf substrate (20×12 cm) was primarily placed in a container and immersed in PIP/water solution for 3 min. Extra aqueous solution was gently removed by a rubber roller. Then, 0.1 wt.% TMC/hexane solution was poured onto the PIP impregnated PSf substrate to initiate IP reaction and maintained for 1 min. The resulting NF membrane was thoroughly rinsed with *n*-hexane and thermal cured in a 60℃-water bath for 10 min. The obtained membranes were then stored in DI water at 4 ℃ overnight. The prepared membranes without and with varied concentrations of polyelectrolyte additive were named as TFC and TFC-P_n, respectively, where *n* denoted to the mass concentrations of the PSSNa additive in aqueous phase solutions.

2.3. Membrane characterization

Before all the measurements, membrane samples were thoroughly vacuum dried. Membrane surface was sputter-coated with a thin layer of gold and platinum. Field-emission scanning electron microscopy (FE-SEM, LEO 1530, UK) was performed using an accelerating voltage of 5.0 kV for the surface morphologies imaging. Transmission electron microscopy (TEM, Philips CM100) was applied to obtain microphotographs from cross-sections of the membrane specimens following the procedures reported in our previous study [32]. The thickness of polyamide layer was measured using ImageJ. Briefly, an Ultracut Eultramicrotome (Reichert, Inc. Depew) was used for sectioning the resin (Epon, Ted Pella) embedded TEM specimens with a thickness of approximately 100 nm. TEM measurements were performed at an accelerating voltage of 100 kV. The topological images and membrane surface roughness were obtained using an atomic force microscopy (AFM) (MultiMode 8-HR, Bruker). Elemental composition of membrane surface was quantified and analyzed by X-ray photoelectron spectroscopy (XPS, Thermo Fishier Scientific). Fourier transform infrared spectroscopy conjunct with Attenuated total reflection (ATR-FTIR, Nicolet 6700, Thermo Fisher Scientific) was performed for determining membrane surface functional groups over a wavenumber range of 650-4000 cm^{-1}. An electrokinetic analyzer (SurPASS, Anton Paar GmbH) was employed for measuring membrane surface charge properties (i.e., ζ potential). An Optical Tensiometer (Attension Theta, Biolin Scientific) was applied to test membrane surface water contact angle and evaluate its hydrophobicity/hydrophilicity.

2.4. Evaluation of membrane separation performance

Membrane separation performance, including water permeance and solutes rejection, was evaluated using a lab-scale cross-flow NF filtration setup. Briefly, a membrane coupon with an effective filtration area of 8 cm^2 was placed in a tailored stainless-steel filtration cell and was pre-compacted with DI water at an applied pressure of 6 bar for 1 h. The cross-flow

183 velocity was set at 7 cm/s. The pure water flux was then measured by weighing the mass of
184 the permeate water collected over a specified time interval based on Eq. (1):

185 $$J_w = \frac{\Delta m}{\Delta t \times A \times \rho} \quad (1)$$

186 where J_w (L m^{-2} h^{-1}) represents the water flux, Δt (h) is the filtration time interval, A (m^2) is
187 the effective membrane area, ρ is the water density, and Δm (kg) is the permeate mass.

188 A series of inorganic salts (i.e., NaCl, Na_2SO_4, $MgCl_2$, $CaCl_2$, and $MgSO_4$, 1000 ppm) were
189 used to prepare feed solutions for salt rejection measurements. The concentrations of the
190 feed (C_f) and the permeate (C_p) solutions were converted from the corresponding
191 conductivity values which were measured using a portable four-electrode conductivity meter
192 (Ultrameter II, Myron L). Salt rejection (R) was calculated based on Eq. (2):

193 $$R = \left(1 - \frac{C_p}{C_f}\right) \times 100\% \quad (2)$$

194 Water permeance (A) and salt permeance (B) were calculated based on Eq. (3) and Eq. (4),
195 respectively:

196 $$A = \frac{J_w}{\Delta P - \Delta \pi} \quad (3)$$

197 $$B = \frac{1 - R}{R} J_w \quad (4)$$

198 Where ΔP (bar) is the applied transmembrane hydraulic pressure, $\Delta \pi$ (bar) is the osmotic
199 pressure difference across the membrane between feed and permeate solution.
200 The separation factor (α) for $CaCl_2$/Na_2SO_4 was determined according to Eq. (5):

201 $$\alpha = \frac{\left(C_{CaCl_2}/C_{Na_2SO_4}\right)_p}{\left(C_{CaCl_2}/C_{Na_2SO_4}\right)_f} = \frac{1 - R_{CaCl_2}}{1 - R_{Na_2SO_4}} \quad (5)$$

202 Neutral organic solutes filtration experiments were performed to determine the log-normal
203 pore size distribution and average membrane pore radius [33]. The feed solution contained
204 a single type of representative neutral organic (i.e., D-Glucose, D-raffinose, dextran, and

dextran, 200 ppm) was prepared. The concentrations of neutral organic molecules were measured using a TOC analyzer (Aurora 1030W, OI Analytical).

The rejection of PFOS was tested using a feed solution containing 200 ppb of PFOS. Before measurements, membrane coupons were first pre-compacted with testing solution for 12 h to obtain a stable water flux and achieve sorption equilibrium. Then, an liquid chromatography coupled with a mass spectrometer (LC-MS) was applied for analyzing the PFOS concentrations in the feed and permeate samples [14]. The PFOS rejection was calculated by measuring the concentrations of PFOS in the feed (C_f) and permeate (C_p) based on Eq.(2).

2.5. Fouling experiments

Fouling experiments were conducted on the control TFC and TFC-P_6 membranes to evaluate their biofouling propensity. *Pseudomonas aeruginosa* (PA14) was used as the model bacterium to induce biofilm formation. Briefly, a single colony of PA14 was picked and incubated in a tryptone soy broth (10 mL) at 170 rpm overnight at 37 ℃. Then, the liquid culture was centrifuged to obtain PA14 suspension which was further washed twice using phosphate buffer solution [34].

Biofouling experiment was carried out with a bench scale cross-flow NF filtration system. The effective filtration area was 7.84 cm^2 [35]. Synthetic wastewater was prepared according to the previous study and was used as the feed solution [36]. After rigorous cleaning and sterilization, the feed solution was circulated by a high-pressure pump at a flow rate of 0.5 L/min. First, the baseline of membrane water flux was established by performing a filtration experiment using the feed stream without bacteria for 24 h. Afterwards, PA14 suspension

was spiked into the feed solution to obtain a bacterial concentration of approximately 10^7 CFU/mL and initiate membrane biofouling. The initial water flux was maintained at 60-70 L $m^{-2} h^{-1}$ by adjusting the applied pressure. After completing biofouling tests, the membrane coupons were carefully removed from the filtration device. The biofilm formed on the membrane surface was stained with DAPI and observed by confocal laser scanning microscopy (CLSM) (LSM700, Carl Zeiss, Jena, Germany) according to our previous studies [37, 38].

3. Results and discussion

3.1. Membrane characterization

SEM analysis was employed to visualize the surface morphological features of all the fabricated membranes (Supplementary Information, Fig. S1). The results demonstrate that both TFC and TFC-P_n membranes had typical nodular-like structures that are generally observed for TFC NF membranes with PIP/TMC chemistry [39]. It is in good agreement with the ATR-FTIR spectra that the higher peak intensity at 1620 cm^{-1} corresponds to amide bonds (C=O) (Supplementary Information, Fig. S5(a)). TEM characterization was also performed on the control TFC and TFC-P_6 membranes to comparatively investigate their cross-sectional micrographs (Fig. 3(a-b), Fig. 3(d-e)). The TFC membrane featured a relatively thin polyamide rejection layer with small discrete nodular-like structures (Fig. 3(a, b)), which is consistent with the SEM observation (Supplementary Information, Fig. S1) [39]. While the polyelectrolyte (i.e., 6 wt.% PSSNa) regulated IP reaction leads to the formation of a PA rejection layer with clearly thicker cross-section (e.g., from an averaged thickness of about 12.4 nm to 21.7 nm) and smoother surface (Fig. 3(d, e)). To further validate the changes on the surface roughness of PA layer, AFM test was employed and confirmed a slightly decreased roughness of TFC-P_6 (with a root mean square roughness (R_q) of 6.0 ± 0.7 nm) compared to TFC (with R_q of 9.2 ± 1.2 nm) (Fig. 3(c, f)). To further understand the underlying mechanism governing the polyelectrolyte assisted IP reaction, the PIP monomer storage within the substrate was measured versus time to investigate its diffusion behavior (Supplementary Information, Fig. S2) [40]. The prohibited diffusion of PIP can be ascribed to the increased viscosity of aqueous phase solution after adding polyelectrolyte and the enhanced electrostatic interaction between the positively charged PIP and negatively charged polyelectrolyte.

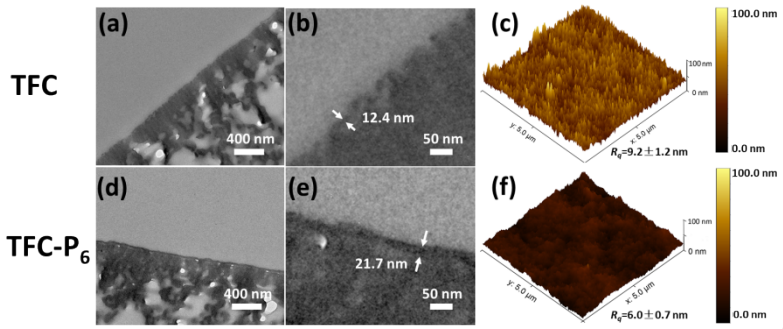

Fig. 3. Membrane characterization of the control TFC and TFC-P_6 membrane fabricated with and without polyelectrolyte additive (i.e., 6 wt.% PSSNa) during interfacial polymerization, respectively. (a) and (d) TEM cross-sectional micrographs; (b) and (e) High magnification images of polyamide layers; (c) and (f) AFM roughness of membrane top surfaces. The scale bar presented in TEM images is 400 nm for (a, d) and 50 nm for (b, e).

XPS analysis was performed on all the fabricated membranes to investigate the effects of polyelectrolyte additive to the membrane surface chemistry (Supplementary Information, Fig. S3). The control TFC membrane showed an O/N ratio of 1.14 which is in good agreement with the previous reported ratio for a typical polyamide selective layer formed by interfacial polymerization reaction of PIP and TMC (Supplementary Information, Table S1). The O/N ratios of all the TFC-P_n membranes were slightly higher (e.g., 1.22, 1.15, and 1.16 for TFC-$P_{0.2}$, TFC-P_2, and TFC-P_{12}, respectively), except for TFC-P_6 of 1.13, indicating a less crosslinking degree compared to that of TFC [40]. The peak deconvolution results of O 1s XPS spectra further disclosed a moderately decreased percentage of amide N-O=C group in TFC-P_n at a binding energy (BE) of ~530.5 eV (i.e., 77.6-79.8%) compared to that of the control TFC (i.e., 82.6%), while the percentage of carboxylic H-O=C group at a BE of ~532.5 eV increased (i.e., from 17.4% for TFC to 20.2-22.4% for TFC-P_n) (Fig. 4). These changes indicated the formation of additional carboxylic group due to the hydrolysis of -COCl functional group (acyl-chloride unit) of TMC, resulting in decreased crosslinking degree and looser structure of the PA layer of TFC-P_n. These changes on membrane surface chemistry were also supported by its lower isoelectric point (Supplementary Information, Fig. S4) (Supplementary Information, Fig. S4), even though the averaged contact angle of

the fabricated membranes maintained a relatively constant value (Supplementary Information, Fig. S5(b)). ATR-FTIR survey exhibited negligible change upon adding polyelectrolyte additive during interfacial polymerization reaction which might be attributed to the relatively low wavenumber resolution.

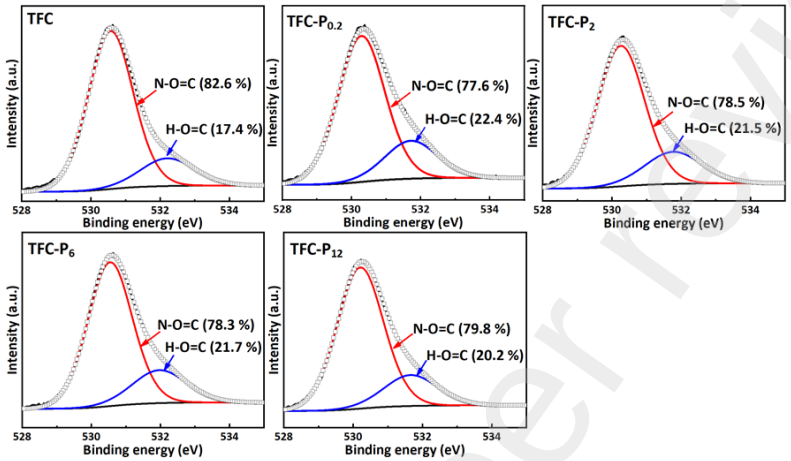

Fig. 4. High-resolution O 1s XPS spectra of (a) the TFC and (b-e) TFC-P_6 membranes were deconvoluted into two components, including amide and carboxyl peak. The peak area percentage of O=C−N (BE of~531.2 eV) and O=C−O (BE of ~533.3 eV) groups were presented.

3.2. Membrane separation properties

Membrane filtration experiments were performed to analyze the effect of polyelectrolyte additive on the separation properties of the resulted PA layer. The separation performance of all the fabricated membranes (TFC and TFC-P_n) was presented in Fig. 5. Specifically, the water permeance of TFC-$P_{0.2}$ was lower than the control TFC membrane which can be well explained by the thicker polyamide layer and thus increased water transport resistance (as discussed in section 3.1). With increasing the concentrations of polyelectrolyte additive, the water permeances of TFC-$P_{0.2}$ and TFC-P_6 further increased and reached 15.7 ± 1.7 L m^{-2} h^{-1} bar^{-1} and 21.8 ± 0.7 L m^{-2} h^{-1} bar^{-1}, respectively. The water permeance was maximized at TFC-P_6 which was about 50% higher than that of the control TFC membrane (14.5 ± 0.2 L m^{-2} h^{-2} bar^{-1}, Fig. 5(a)). The advanced water permeance of both TFC-$P_{0.2}$ and TFC-P_6 can

be attributed to the looser structure of polyamide layer which outweigh the negative effects of their increased thickness. In addition, TFC-P_6 demonstrated an obviously lower rejection of neutral solutes than the control TFC (Supplementary Information, Fig. S6) which further supported the reduced size exclusion effects of the PA rejection layer of TFC-P_6 and thereby larger mean pore size than that of control TFC (i.e., a mean pore radius $r_p \approx 0.6$ nm for TFC-P_6 and $r_p \approx 0.43$ nm for TFC) (Supplementary Information, Fig. S7). According to these rejection results, the log-normal pore size distribution of the TFC and TFC-P_6 membranes were determined. Besides, TFC-P_{12} demonstrated a substantially lower water permeance of 13.3 ± 1.9 L m^{-2} h^{-1} bar^{-1} that additional polyelectrolyte in aqueous solution during IP reaction would adversely increase water transport resistance.

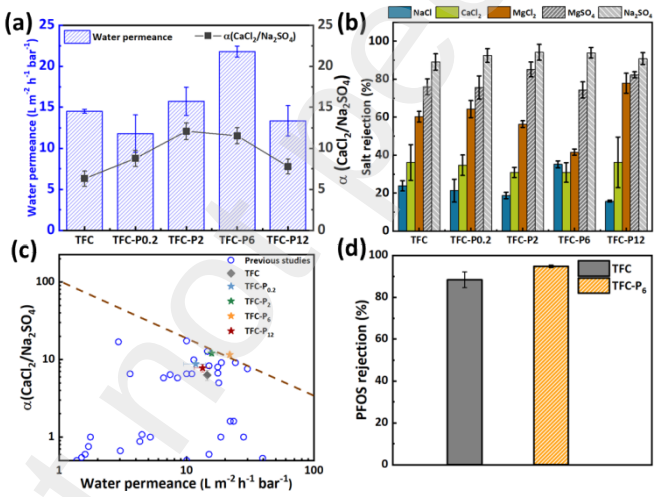

Fig. 5. Membrane separation performances of TFC and TFC-P_n membranes. (a) Water permeance and $CaCl_2/Na_2SO_4$ selectivity, (b) Salt rejection of five different kinds of salts (i.e., NaCl, $CaCl_2$, $MgCl_2$, $MgSO_4$, and Na_2SO_4). Other testing conditions are as following: feed solution contained 1000 ppm of each salt; hydraulic pressure of 6 bar, crossflow velocity of 7 cm/s. (c) Trade-off relationship between $CaCl_2/Na_2SO_4$ selectivity and water permeance based on the previous publications on TFC NF membranes while a dash upper bound line was represented for the separation performance. (d) Rejection of PFOS in DI water of the control TFC and TFC-P_6 membranes.

In spite of the changes on water permeance, TFC-P_n membranes maintained high rejection of salts containing multivalent anions (e.g., $MgSO_4$ and Na_2SO_4), due to the Donnan

exclusion effect of the negatively charged membrane surface on SO_4^{2-} and its relatively large hydrated ionic radius (i.e., about 3.79 angstrom for SO_4^{2-}) (Fig. 5(b)), resulting in high water/solute (e.g., A/B_{Na2SO4}) (Supplementary Information, Fig. S8). In consideration of the enlarged mean pore size of TFC-P_n, its electrostatic exclusion effect dominated over its size exclusion effect. For salts containing multivalent cation, TFC-P_2 and TFC-P_6 demonstrated slightly decreased rejection (e.g., $MgCl_2$ and $CaCl_2$ rejection of 41.6 ± 2% and 30.9 ± 5% for TFC-P_6) compared to the control TFC (e.g., $MgCl_2$ and $CaCl_2$ rejection of 60.3 ± 3% and 31.6 ± 12%). It can be possibly ascribed to the enhanced electrostatic interaction between the additional surface negative charge of TFC-P_6 and multivalent cations, as well as the looser structure of polyamide layer. Consequently, TFC-P_n illustrated enhanced selectivity between calcium and sulfate ions, the effectiveness of which can be well evaluated by the separation factor ($\alpha = B_{(CaCl2)}/B_{(Na2SO4)}$) (Fig. 5(a)). This coefficient has been widely applied to quantify the solute-solute selectivity of specific membranes [39]. For example, the selectivity of TFC-P_6 showed the highest α value of 11.5 ± 1.0 compared to 6.3 ± 0.9 for the control TFC. We further investigated the $CaCl_2/Na_2SO_4$ selectivity of polyamide thin film composite NF membranes reported in the previous publications. As illustrated in Fig. 5(c), there is a clear trade-off relationship between the selectivity coefficient α and water permeance for the reported NF membranes based on PA chemistry in the literatures that an upper bound line can be recognized in the Fig. 5(c). Compared to the previous reported NF membranes and the control TFC fabricated in this study, TFC-P_6 outperformed the rest in the separation performance.

A high α value would be beneficial to practical implementation of NF process, especially in groundwater treatment, for the reduced scaling risks and the enhanced permeate recovery[8]. In addition, the well retained essential minerals (e.g., Ca^{2+}, Mg^{2+}) within the treated

groundwater of TFC-P_n would be good for human health and made treated groundwater more favorable for drinking water resource. The low permeance of multivalent cations and simultaneously improved water permeance of TFC-P_n can also minimize the osmotic pressure penalty across the membrane, thus reducing hydraulic pump energy consumption. Accordingly, the operation and maintenance cost (e.g., chemical cleaning cost) can be reduced. Furthermore, for groundwater contaminated with emergent contaminants (e.g., PFOS which has been widely detected in natural water resources), the contaminant rejection of TFC-P_6 membrane (94.8%) was significantly higher than that of the control TFC (88.3%), thanks to its large hydrated radius and its electrostatic interaction with the additional negative charge on membrane surface (Fig. 5(d)).

3.3. The fouling behavior of TFC-P_n membranes

The biofouling behavior of the control TFC and TFC-P_n (using TFC-P_6 as an example) are comparatively studied. The normalized water flux (J_w/J_0) of both TFC and TFC-P_n with and without the presence of biomass in the feed streams were curved versus time during the experiments (Fig. 6(a)). The initial flux of all the tests, including baseline and fouling measurements, was set at about 60-70 L m^{-2} h^{-1} by adjusting operation pressure and was recorded as J_0. Despite the well-controlled baseline of both TFC and TFC-P_6, their fouling trends were different. At the beginning, TFC and TFC-P_6 demonstrated a similar and steadily declined water flux. Subsequently, the decline rate of permeate flux of TFC-P_6 increased 8 hours later, while the control TFC suffered a more dramatic decline in permeate flux. The flux variation of TFC is consistent with previous reported fouling curves that the sudden decline of permeate flux can be attributed to the formation of biofilm cake layer on the membrane surface [41]. The bacteria were initially attached onto the membrane which was facilitated by the surface hydrophobic interaction of TFC and microorganism, and were

subsequently anchored by the extracellular organic compounds (e.g., EPS), leading to the microbial colonization and biofilm formation. A layer of biofilm on the control TFC can be recognized in CLSM images (Fig. 6(b)). In the contrary, compared to the control TFC, TFC-P_6 was less prone to biofouling that its water flux can be better maintained. It can be possibly due to the enhanced electrostatic exclusion of negatively charged bacteria by the additional negative charges on the membrane surface of TFC-P_6, resulting in an anti-fouling performance. Moreover, its smoother surface morphology would restrict the adhesion of biofilm on the membrane surface. Finally, the CLSM micrographs of TFC-P_6 membrane surface exhibited less biofoulant deposition and confirmed its anti-biofouling performance (Fig. 6(c)).

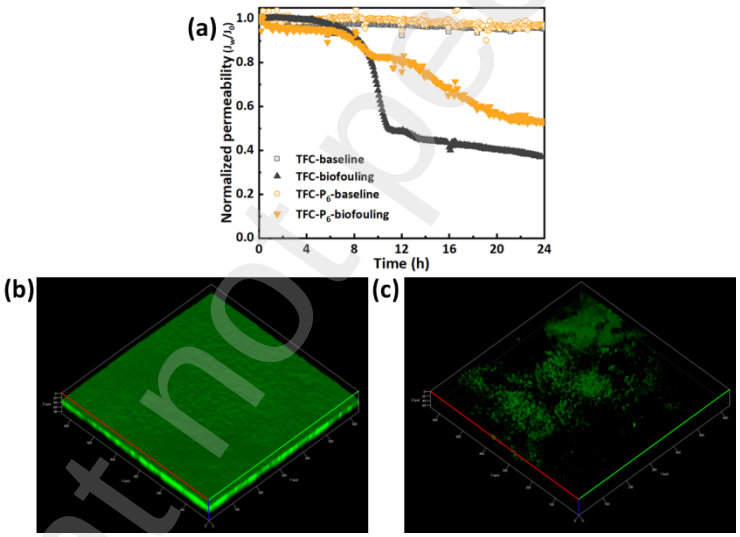

Fig. 6. Anti-biofouling tests of TFC and TFC-P_6 membrane with a cross-flow nanofiltration system. (a)Normalized water flux versus time after 24 h filtration at 6 bar. CLSM images of TFC(b) and TFC-P_6 membrane after 24 h filtration.

4. Conclusions

In this study, we proposed a simple method of using polyelectrolyte as an aqueous phase additive to regulate the interfacial polymerization reaction. A negatively charged PSS was selected as the model additive of PIP aqueous phase solution to tune the formation of PA

layer toward better selectivity and anti-biofouling behavior. The results shown that the diffusion of amine monomer into the organic phase solution was confined by its electrostatic interaction with polyelectrolyte, leading to a PA layer with reduced degree of cross-linking and increased density of surface negative charges. Using a moderate concentration of polyelectrolyte additive, TFC-P_6 demonstrated enhanced water permeance and better selectivity for calcium chloride over sodium sulfate, and improved anti-fouling performance compared to the control TFC.

Both the selectivity of water/solute (e.g., A/B_{Na2SO4}) and that of different solutes (e.g., B_{CaCl2}/B_{Na2SO4}) are critical parameters for NF membranes. A high selectivity for water over salt (i.e., high A/B_{Na2SO4} ratio) would be beneficial to the quality of purified water product, while a high calcium chloride-sodium sulfate selectivity (i.e., high B_{CaCl2}/B_{Na2SO4} ratio) would be favorable for decreasing membrane scaling potential and reducing pressure energy consumption. In addition, the well retained mineral ions (e.g., Ca^{2+}, Mg^{2+}) within the permeate would make it more suitable for drinking purpose. Furthermore, TFC-P_6 showed a higher rejection of emergent pollutant thanks to the combined size exclusion effect and enhanced electrostatic interaction. Due to the significant health risks of PFOS, the current study provides us a facile approach to tune the formation of PA rejection layer and fabricate NF membranes with simultaneously production of high-quality water in groundwater treatment. The critical roles of polyelectrolyte additive in enhancing membrane separation performance and antifouling properties was investigated. Future studies need to be performed to further explore the impact of the molecular structure and charge density of polyelectrolyte additive on the interfacial polymerization reaction and the formation of PA layer.

Acknowledgements

The work was substantially supported by a grant from the Innovation and Technology Fund (ITS/249/20) of the Hong Kong SAR, China. The authors also acknowledge the financial support from Beijing Normal University.

References

[1] C. Wei, Q. Wang, X. Song, X. Chen, R. Fan, D. Ding, Y. Liu, Distribution, source identification and health risk assessment of PFASs and two PFOS alternatives in groundwater from non-industrial areas, Ecotoxicol Environ Saf, 152 (2018) 141-150.

[2] M. Patel, R. Kumar, K. Kishor, T. Mlsna, C.U. Pittman, D. Mohan, Pharmaceuticals of Emerging Concern in Aquatic Systems: Chemistry, Occurrence, Effects, and Removal Methods, Chem. Rev., 119 (2019) 3510-3673.

[3] I. Ross, J. McDonough, J. Miles, P. Storch, P. Thelakkat Kochunarayanan, E. Kalve, J. Hurst, S. S. Dasgupta, J. Burdick, A review of emerging technologies for remediation of PFASs, Remediation Journal, 28 (2018) 101-126.

[4] L. Charuaud, E. Jarde, A. Jaffrezic, M.F. Thomas, B. Le Bot, Veterinary pharmaceutical residues from natural water to tap water: Sales, occurrence and fate, J Hazard Mater, 361 (2019) 169-186.

[5] Y. Luo, W. Guo, H.H. Ngo, L.D. Nghiem, F.I. Hai, J. Zhang, S. Liang, X.C. Wang, A review on the occurrence of micropollutants in the aquatic environment and their fate and removal during wastewater treatment, Sci Total Environ, 473-474 (2014) 619-641.

[6] H. Guo, R. Dai, M. Xie, L.E. Peng, Z. Yao, Z. Yang, L.D. Nghiem, S.A. Snyder, Z. Wang, C.Y. Tang, Tweak in Puzzle: Tailoring Membrane Chemistry and Structure toward Targeted Removal of Organic Micropollutants for Water Reuse, Environ Sci Technol Lett., 9 (2022) 247-257.

[7] S. Hurley, E. Houtz, D. Goldberg, M. Wang, J.-S. Park, D.O. Nelson, P. Reynolds, L. Bernstein, H. Anton-Culver, P. Horn-Ross, M. Petreas, Preliminary Associations between the Detection of Perfluoroalkyl Acids (PFAAs) in Drinking Water and Serum Concentrations in a Sample of California Women, Environ Sci Technol Lett., 3 (2016) 264-269.

[8] C. Boo, Y. Wang, I. Zucker, Y. Choo, C.O. Osuji, M. Elimelech, High Performance Nanofiltration Membrane for Effective Removal of Perfluoroalkyl Substances at High Water Recovery, Environ. Sci. Technol., 52 (2018) 7279-7288.

[9] S.P. Lenka, M. Kah, L.P. Padhye, A review of the occurrence, transformation, and removal of poly- and perfluoroalkyl substances (PFAS) in wastewater treatment plants, Water Res, 199 (2021) 117187.

[10] R. Loos, B.M. Gawlik, G. Locoro, E. Rimaviciute, S. Contini, G. Bidoglio, EU-wide survey of polar organic persistent pollutants in European river waters, Environ. Pollut., 157 (2009) 561-568.

[11] R. Loos, R. Carvalho, D.C. Antonio, S. Comero, G. Locoro, S. Tavazzi, B. Paracchini, M. Ghiani, T. Lettieri, L. Blaha, B. Jarosova, S. Voorspoels, K. Servaes, P. Haglund, J. Fick, R.H. Lindberg, D. Schwesig, B.M. Gawlik, EU-wide monitoring survey on emerging polar organic contaminants in wastewater treatment plant effluents, Water Res, 47 (2013) 6475-6487.

[12] C. Kunacheva, S. Fujii, S. Tanaka, S.T. Seneviratne, N.P. Lien, M. Nozoe, K. Kimura, B.R. Shivakoti, H. Harada, Worldwide surveys of perfluorooctane sulfonate (PFOS) and perfluorooctanoic acid (PFOA) in water environment in recent years, Water Sci Technol, 66 (2012) 2764-2771.

[13] J.W. Martin, M.M. Smithwick, B.M. Braune, P.F. Hoekstra, D.C. Muir, S.A. Mabury, Identification of long-chain perfluorinated acids in biota from the Canadian Arctic, Environ Sci Technol, 38 (2004) 373-380.

[14] H. Guo, J. Zhang, L.E. Peng, X. Li, Y. Chen, Z. Yao, Y. Fan, K. Shih, C.Y. Tang, High-Efficiency Capture and Recovery of Anionic Perfluoroalkyl Substances from Water Using

PVA/PDDA Nanofibrous Membranes with Near-Zero Energy Consumption, Environ Sci Technol Lett., 8 (2021) 350-355.
[15] X. Dauchy, V. Boiteux, C. Bach, A. Colin, J. Hemard, C. Rosin, J.F. Munoz, Mass flows and fate of per- and polyfluoroalkyl substances (PFASs) in the wastewater treatment plant of a fluorochemical manufacturing facility, Sci Total Environ, 576 (2017) 549-558.
[16] Q. Yu, R. Zhang, S. Deng, J. Huang, G. Yu, Sorption of perfluorooctane sulfonate and perfluorooctanoate on activated carbons and resin: Kinetic and isotherm study, Water Res, 43 (2009) 1150-1158.
[17] D. Lu, S. Sha, J. Luo, Z. Huang, X. Zhang Jackie, Treatment train approaches for the remediation of per- and polyfluoroalkyl substances (PFAS): A critical review, J Hazard Mater, 386 (2020) 121963.
[18] H. Guo, X. Li, W. Yang, Z. Yao, Y. Mei, L.E. Peng, Z. Yang, S. Shao, C.Y. Tang, Nanofiltration for drinking water treatment: a review, Front. Chem. Sci. Eng., (2021) 1-18.
[19] R. Rattanaoudom, C. Visvanathan, Removal of PFOA by hybrid membrane filtration using PAC and hydrotalcite, Desalination Water Treat., 32 (2011) 262-270.
[20] V. Boiteux, X. Dauchy, C. Bach, A. Colin, J. Hemard, V. Sagres, C. Rosin, J.F. Munoz, Concentrations and patterns of perfluoroalkyl and polyfluoroalkyl substances in a river and three drinking water treatment plants near and far from a major production source, Sci Total Environ, 583 (2017) 393-400.
[21] A. Soriano, D. Gorri, A. Urtiaga, Efficient treatment of perfluorohexanoic acid by nanofiltration followed by electrochemical degradation of the NF concentrate, Water Res, 112 (2017) 147-156.
[22] K.U. Goss, The pKa values of PFOA and other highly fluorinated carboxylic acids, Environ Sci Technol, 42 (2008) 456-458.
[23] J. Xiong, Y. Hou, J. Wang, Z. Liu, Y. Qu, Z. Li, X. Wang, The rejection of perfluoroalkyl substances by nanofiltration and reverse osmosis: influencing factors and combination processes, Environ. Sci.: Water Res. Technol., 7 (2021) 1928-1943.
[24] A.W. Mohammad, Y.H. Teow, W.L. Ang, Y.T. Chung, D.L. Oatley-Radcliffe, N. Hilal, Nanofiltration membranes review: Recent advances and future prospects, Desalination, 356 (2015) 226-254.
[25] P. Wang, F. Wang, H. Jiang, Y. Zhang, M. Zhao, R. Xiong, J. Ma, Strong improvement of nanofiltration performance on micropollutant removal and reduction of membrane fouling by hydrolyzed-aluminum nanoparticles, Water Res, 175 (2020) 115649.
[26] F. Beyer, B.M. Rietman, A. Zwijnenburg, P. van den Brink, J.S. Vrouwenvelder, M. Jarzembowska, J. Laurinonyte, A.J.M. Stams, C.M. Plugge, Long-term performance and fouling analysis of full-scale direct nanofiltration (NF) installations treating anoxic groundwater, J. Membr. Sci., 468 (2014) 339-348.
[27] W. Yang, L. Long, H. Guo, C. Wu, S. Zhou, Y. Mei, L.E. Peng, W. Liu, Z. Yang, W. Li, C.Y. Tang, Facile synthesis of nanofiltration membrane with asymmetric selectivity towards enhanced water recovery for groundwater remediation, J. Membr. Sci., 663 (2022).
[28] Z. Tan, S. Chen, X. Peng, L. Zhang, C. Gao, Polyamide membranes with nanoscale turing structures for water purification, Science, 360 (2018) 518-521.
[29] L.E. Peng, Z. Yao, X. Liu, B. Deng, H. Guo, C.Y. Tang, Tailoring Polyamide Rejection Layer with Aqueous Carbonate Chemistry for Enhanced Membrane Separation: Mechanistic Insights, Chemistry-Structure-Property Relationship, and Environmental Implications, Environ. Sci. Technol., 53 (2019) 9764-9770.
[30] Z. Yao, H. Guo, Z. Yang, W. Qing, C.Y. Tang, Preparation of nanocavity-contained thin film composite nanofiltration membranes with enhanced permeability and divalent to monovalent ion selectivity, Desalination, 445 (2018) 115-122.

[31] L.E. Peng, Z. Yao, Z. Yang, H. Guo, C.Y. Tang, Dissecting the Role of Substrate on the Morphology and Separation Properties of Thin Film Composite Polyamide Membranes: Seeing Is Believing, Environ. Sci. Technol., 54 (2020) 6978-6986.
[32] Z. Yang, H. Guo, Z.-k. Yao, Y. Mei, C.Y. Tang, Hydrophilic Silver Nanoparticles Induce Selective Nanochannels in Thin Film Nanocomposite Polyamide Membranes, Environ. Sci. Technol., 53 (2019) 5301-5308.
[33] Z. Yang, F. Wang, H. Guo, L.E. Peng, X.H. Ma, X.X. Song, Z. Wang, C.Y. Tang, Mechanistic Insights into the Role of Polydopamine Interlayer toward Improved Separation Performance of Polyamide Nanofiltration Membranes, Environ. Sci. Technol., 54 (2020) 11611-11621.
[34] P.-F. Sun, Y. Jang, S.-Y. Ham, H. Ryoo, H.-D. Park, Effects of reverse solute diffusion on membrane biofouling in pressure-retarded osmosis processes, Desalination, 512 (2021) 115145.
[35] L. Wang, D. Rehman, P.-F. Sun, A. Deshmukh, L. Zhang, Q. Han, Z. Yang, Z. Wang, H.-D. Park, J.H. Lienhard, C.Y. Tang, Novel Positively Charged Metal-Coordinated Nanofiltration Membrane for Lithium Recovery, ACS Appl. Mater. Interfaces, 13 (2021) 16906-16915.
[36] P.-F. Sun, T.-S. Kim, H.-S. Kim, S.-Y. Ham, Y. Jang, Y.-G. Park, C.Y. Tang, H.-D. Park, Improved anti-biofouling performance of pressure retarded osmosis (PRO) by dosing with chlorhexidine gluconate, Desalination, 481 (2020).
[37] K.-H. Park, P.-F. Sun, E.H. Kang, G.D. Han, B.J. Kim, Y. Jang, S.-H. Lee, J.H. Shim, H.-D. Park, Photocatalytic anti-biofouling performance of nanoporous ceramic membranes treated by atomic layer deposited ZnO, Sep. Purif. Technol., 272 (2021) 118935.
[38] K.-H. Park, P.-F. Sun, E.H. Kang, G.D. Han, B.J. Kim, Y. Jang, S.-H. Lee, J.H. Shim, H.-D. Park, Photocatalytic anti-biofouling performance of nanoporous ceramic membranes treated by atomic layer deposited ZnO, Sep. Purif. Technol., 272 (2021).
[39] Z. Yang, Z.W. Zhou, H. Guo, Z. Yao, X.H. Ma, X. Song, S.P. Feng, C.Y. Tang, Tannic Acid/Fe(3+) Nanoscaffold for Interfacial Polymerization: Toward Enhanced Nanofiltration Performance, Environ. Sci. Technol., 52 (2018) 9341-9349.
[40] X. You, K. Xiao, H. Wu, Y. Li, R. Li, J. Yuan, R. Zhang, Z. Zhang, X. Liang, J. Shen, Z. Jiang, Electrostatic-modulated interfacial polymerization toward ultra-permselective nanofiltration membranes, iScience, 24 (2021) 102369.
[41] Y. Gu, Y.N. Wang, J. Wei, C.Y. Tang, Organic fouling of thin-film composite polyamide and cellulose triacetate forward osmosis membranes by oppositely charged macromolecules, Water Res, 47 (2013) 1867-1874.

Supplementary Information

Polyelectrolyte assisted interfacial polymerization for polyamide nanofiltration membrane with enhanced separation and anti-biofouling properties in groundwater treatment

Ying Mei[a,b] *, Zhe Yang[b], Peng-Fei Sun[b,c], Shenghua Zhou[b], Hao Guo[b], Lu Elfa Peng[b], Zhikan Yao[b,d], Wulin Yang[b,e], Chuyang Y. Tang[b]

[a]*Research and Development Center for Watershed Environmental Eco-Engineering, Advanced Institute of Natural Sciences, Beijing Normal University, Zhuhai 519087, PR China*

[b]*Department of Civil Engineering, The University of Hong Kong, Pokfulam, Hong Kong SAR, China*

[c]*School of Civil, Environmental and Architectural Engineering, Korea University, Seoul 02841, South Korea*

[d]*MOE Engineering Research Center of Membrane and Water Treatment Technology, College of Chemical and Biological Engineering, Zhejiang University, Hangzhou 310027, PR China*

[e]*College of Environmental Sciences and Engineering, Peking University, Beijing 100871, PR China*

* Corresponding author address:

B504 Muduo Building, Beijing Normal University, Zhuhai,18 Jinfeng Road, Zhuhai, Guangdong, China.

25 *Tel: (+86) 15034117623;*

26 *E-mail address: meiying@bnu.edu.cn (Ying Mei)*

S1. Microscopic images of membrane top surfaces

SEM microscopic characterization was performed on the control TFC membrane and TFC-P_n membranes. All the membrane surfaces have representative nodular-like nanostructures of polyamide rejection layer based on PIP/TMC chemistry. In addition, with increasing the mass concentration of polyelectrolyte additive in the aqueous solution (e.g., from TFC-$P_{0.2}$ to TFC-P_6), the corresponding surface morphology remained almost the same except there are emerging fragments in the top view of TFC-P_6. Therefore, adding negatively charged polyelectrolytes in the aqueous phase solution tend to have neglected effect on the surface morphologies of TFC NF membranes.

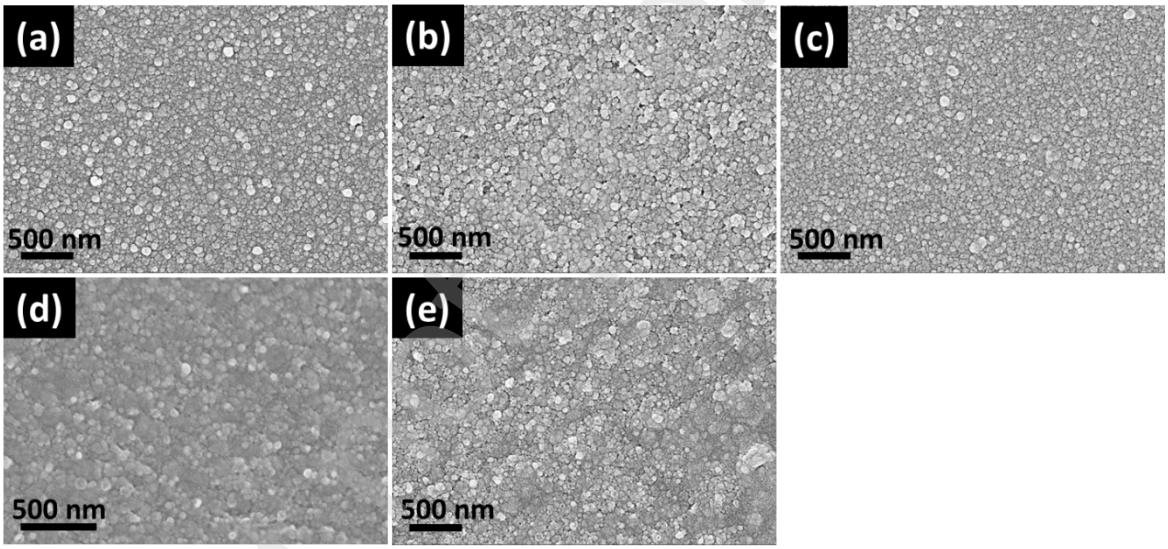

Fig. S1. SEM micrographs (plan views) of (a) the control TFC membrane and (b-e) the TFC-P_n membranes fabricated by the PIP aqueous phase solution with various concentrations (0.2, 2, 6, 12 wt.%) of PSSNa additive. The scale bar for all the images is 500 nm.

S2. Measurements of PIP diffusion behavior

PIP diffusion experiments were conducted to evaluate the electrostatic interaction between negatively charged polyelectrolyte and positively charged amine aqueous phase monomer during interfacial polymerization (IP) reaction. The experimental procedures were adapted

from the IP reaction based on a previous study[1]. Specifically, PES substrate was immersed in PIP aqueous phase solution for 3 min and was subsequently immersed in a fixed volume (e.g., 20 mL) of pure hexane after thoroughly removing the excess PIP solution by a rubber roller. Meanwhile, 1.5 mL organic solution was extracted each time to detect the PIP concentration by UV-vis spectroscopy at predetermine time interval (i.e., 0, 5, 10, 30 min). The diffusion rate of PIP was obviously quicker for aqueous solution without any additive compared to that with negatively charged polyelectrolyte, as shown in Fig. B1. With increasing the concentration of PSSNa in aqueous phase solution, the PIP diffusion was further prohibited (e.g., from 0.12 and 0.15 mmol/L for TFC-$P_{0.2}$ and TFC-P_2 to 0.08 and 0.10 mmol/L for TFC-P_6 and TFC-P_{12} at 30 min) by its electrostatic interaction with PSSNa of large molecular weight (MW ~70,000) and enhanced solution viscosity.

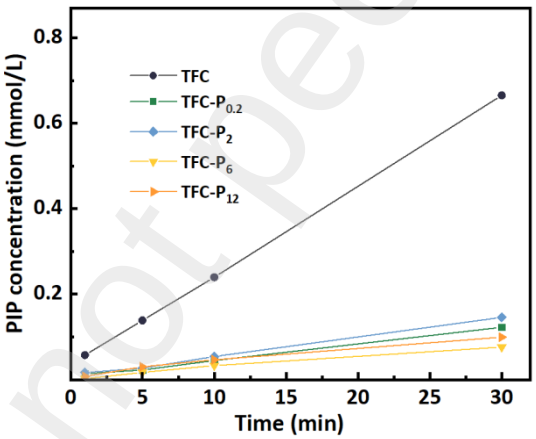

Fig. S2. The concentration of PIP diffusion from the aqueous phase to the organic phase versus time.

S3. Characterization of membrane surface chemistry

We explored surface elemental composition of the TFC and TFC-P_n membranes using XPS technique (Fig. S3 and Table S1). The slight increased O/N ratio of the PA rejection layer of TFC-P_n (e.g., TFC-$P_{0.2}$, TFC-P_2, and TFC-P_{12}) can be explained by its moderately enhanced hydrolysis of acryl chloride group contained in TMC (i.e., decreased cross-linking degree) compared to that of the control TFC. In addition, ζ potential testing was conducted on the

TFC and TFC-P_6 membranes for surface charge characterization (Fig. S4). The shift of isoelectric point (IEP) to the lower pH (i.e., from 4.1 for TFC to 3.4 for TFC-P_6) indicated the presence of additional surface negative charges on TFC-P_6 membrane.

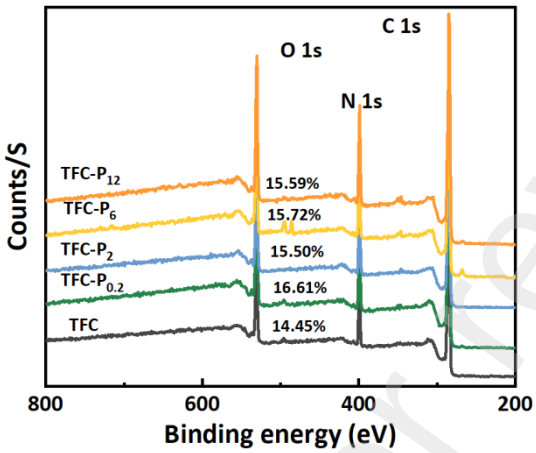

Fig. S3. XPS spectrum of TFC and TFC-P_n membranes.

Table S1. Relative elemental composition (%) of membrane surface analyzed from the XPS measurements of the TFC and TFC-P_n membranes. The O/N ratio was calculated with the atomic percent of O and N.

Membrane	C (%)	O (%)	N (%)	O/N
TFC	72.88	14.45	12.67	1.14
TFC-$P_{0.2}$	69.8	16.61	13.59	1.22
TFC-P_2	71.01	15.5	13.49	1.15
TFC-P_6	70.38	15.72	13.91	1.13
TFC-P_{12}	70.94	15.59	13.47	1.16

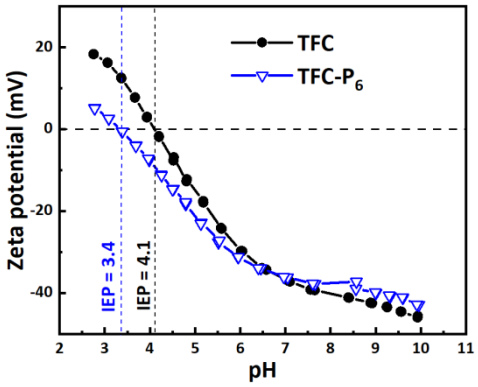

Fig. S4. Zeta potential of TFC and TFC-P_6 membranes. The IEP of each membrane was presented. The tests were performed in a background solution of 10 mM NaCl.

The ATR-FTIR spectra of the TFC and TFC-P_n membranes showed emerging stretching vibration of C=O bonds at 1620 cm^{-1}, confirming the successful formation of polyamide rejection layer. The intensified peak at 1440 cm^{-1} can be ascribed to the O-H bonds of carboxylic group formed by hydrolysis of the acryl chloride groups of TMC. Furthermore, contact angle measurements provided useful information related to the membrane surface hydrophilicity. All the TFC-P_n membranes exhibited moderately better hydrophilicity due to the presence of additional carboxylic groups.

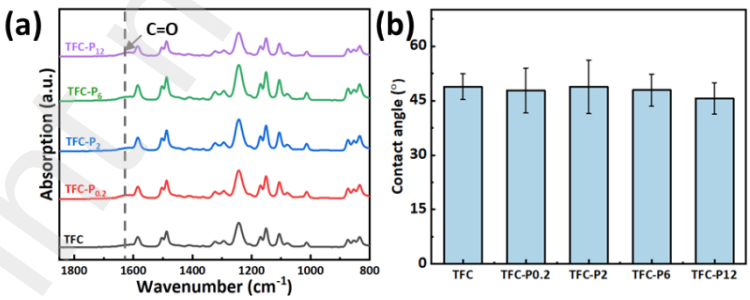

Fig. S5. ATR-FTIR spectra (a) and contact angle (b) of the TFC and TFC-P_n membranes.

S4. Characterization of membrane pore size distribution

Membrane rejection of neutral molecules was explored to evaluate the size exclusion performance of the control TFC and TFC-P_6 (Fig. S6). TFC-P_6 obtained lower rejection of

glucose (MW 180), raffinose (MW 594), and dextran with molecular weight of 1000 compared to the control TFC. Based on neutral molecules rejection, the surface pore radius of membrane samples was calculated. The mean pore size of TFC-P_6 (R_m= 0.6 nm) was effectively larger than that of TFC (R_m= 0.43 nm) (Fig. S7). The larger mean pore size of TFC-P_6 can be attributed to the less cross-linking degree of the polyamide layer.

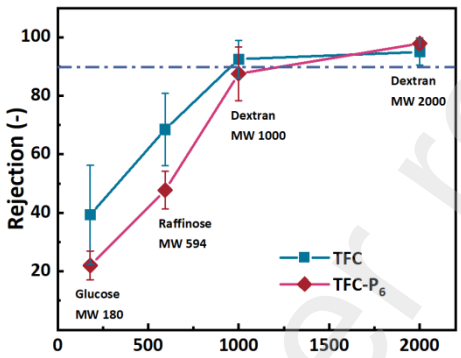

Fig. S6. Neutral molecules rejection for the control TFC and TFC-P_6 membrane using feed solution concentration of 200 ppm.

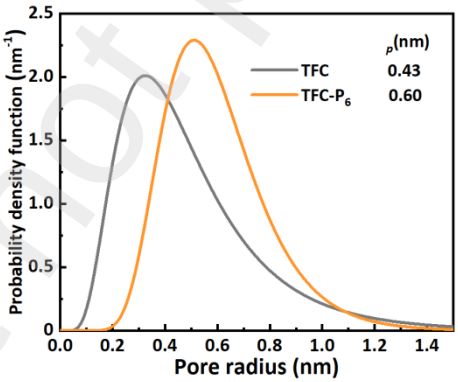

Fig. S7. Pore size distribution and mean pore size of TFC and TFC-P_6 membrane based on rejection results of neutral molecules.

S5. Water permeance-salt selectivity investigation

There is a trade-off relationship between water permeance and NaCl/Na_2SO_4 selectivity for conventional polyamide NF membranes with an upper bound of the separation performance being presented (Fig. S8).

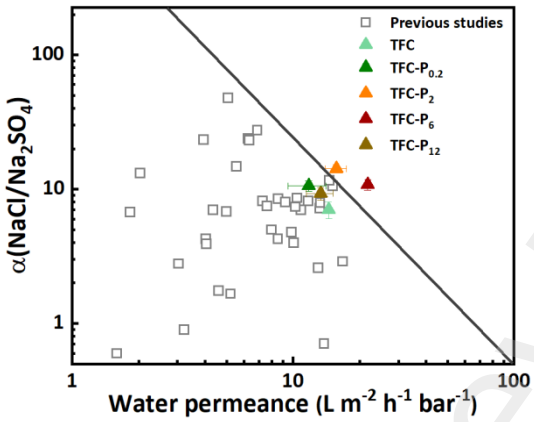

Fig. S8. Trade-off relationship between membrane water permeance and $NaCl/Na_2SO_4$ selectivity based on previous reported studies on polyamide NF membranes. $NaCl/Na_2SO_4$ selectivity was presented as $B(NaCl)/B(Na_2SO_4)$ ratio.

1. You, X.; Xiao, K.; Wu, H.; Li, Y.; Li, R.; Yuan, J.; Zhang, R.; Zhang, Z.; Liang, X.; Shen, J.; Jiang, Z., Electrostatic-modulated interfacial polymerization toward ultra-permselective nanofiltration membranes. *iScience* **2021,** *24*, (4), 102369.